Liquid-crystal phases of self-assembled molecular aggregates

1993 J. Phys.: Condens. Matter 5 2651

(http://iopscience.iop.org/0953-8984/5/17/002)

J. Phys.: Condens. Matter 5 (1993) 2651–2678. Printed in the UK

REVIEW ARTICLE

Liquid-crystal phases of self-assembled molecular aggregates

Mark P Taylor† and Judith Herzfeld‡

† Department of Chemistry, Dartmouth College, Hanover, NH 03755, USA
‡ Department of Chemistry, Brandeis University, Waltham, MA 02254, USA

Received 5 January 1993

Abstract. A variety of molecules reversibly self-assemble in solution, forming non-covalently bonded molecular aggregates. In many cases these aggregates are asymmetric in shape and are observed to form liquid-crystal phases. The nature of and mechanisms for liquid-crystalline ordering in such self-assembled systems is the focus of this review.

Contents

1. Introduction

In certain respects, the lyotropic ordering of molecules in solution is easier to understand than the thermotropic ordering of molecules in neat fluids. This is because the interactions between particles responsible for ordering in concentrated solutions need only be described relative to the interactions of the particles with solvent. As a result, explicit consideration of van der Waals attractions is unnecessary and repulsions between electrically neutral particles can be approximated in most cases by hard-core potentials. For length scales large compared to the characteristic length for solvent structure, the solvent can be considered as

0953-8984/93/172651+28$07.50

a continuum background. The description of a lyotropic system is thus similar to that of a hard-particle fluid [1–3].

This simple picture of particle interactions is fortunate because there is a large class of important lyotropic liquid crystals for which complications arise at another level. These are systems in which the particles are labile and highly polydisperse because they are formed by the open-ended, reversible aggregation of molecules. For example, amphiphilic polyaromatic molecules can reversibly associate to form cylindrical stacks of variable length [4–6]. Analogously, rigid surfactant molecules can reversibly associate to form disc-like aggregates of variable diameter [6–9]. More generally, surfactants can form extended micelles of both rod-like and disc-like geometry [10–16]. Among larger molecules, the so-called polymerizing proteins reversibly assemble into multistranded filaments [17]. These filaments give structure to living cells, and their assembly and disassembly is a vital part of cell growth and cell motion [18].

Reversible assembly introduces new degrees of freedom into the system. In addition to the usual spatial degrees of freedom for rotational and translational ordering, the self-assembling systems have molecular degrees of freedom corresponding to the distribution of aggregate shapes and sizes. All of these degrees of freedom are coupled to each other: steric interactions between particles of various sizes and shapes are responsible for spatial ordering and spatial ordering alters the relative stabilities (i.e. the thermodynamic activities) of particles of different sizes and shapes. Any theory of reversibly assembling lyotropic liquid crystals must take these reciprocal effects into account and consider the joint optimization of all degrees of freedom.

In this review we first discuss the theory of liquid-crystalline ordering in simple monodisperse lyotropic systems (section 2) and the process of aggregate self-assembly in ideal-solution conditions (section 3). We then proceed to develop a general theoretical approach for the description of liquid-crystalline ordering in systems of self-assembled molecular aggregates. In section 4 we present descriptions of orientational ordering in surfactant and protein systems. In section 5 we present descriptions of positional ordering for systems that have been designed to form only rods or discs. In section 6 we consider the strengths and limitations of the present theory, with an assessment of future directions.

2. Entropically driven ordering

As discussed above, the formation of liquid-crystalline phases in lyotropic systems can, to a good approximation, be considered a purely entropic process. This statement implies that the long-range order in liquid crystals, much like the short-range order in simple fluids, can be attributed to hard-core interparticle interactions. Onsager was the first to show that an isotropic–nematic transition is possible in a system of asymmetric hard particles [1]. The mechanism for this entropically driven orientational ordering is a competition between rotational and translational degrees of freedom. Onsager's result suggests an analogous mechanism for entropically driven positional ordering in hard-particle fluids. We have proposed that positionally ordered phases, such as the smectic and columnar, may be stabilized by a trade-off in translational entropy between the three dimensions of the system. A simple cell model has been developed that displays such entropically driven positional ordering [19]. In this section we briefly sketch the Onsager model for entropically driven orientational ordering and our cell model for entropically driven translational ordering. Finally we note that only recently have computer simulation studies been carried out that convincingly demonstrate the existence of both orientational and translational ordering in systems of asymmetric hard particles.

2.1. Onsager model for orientational ordering

The possibility of liquid-crystal ordering in a system of hard particles was first investigated by Onsager, who demonstrated that in a fluid of long rigid hard rods the disordered or isotropic phase, stable at low densities, becomes unstable above a critical density with respect to an orientationally ordered or nematic phase [1]. The Onsager calculation employs a second virial expansion of the free energy and thus is only valid in the dilute limit. However, since the critical transition density is proportional to the inverse square of the rod length, the isotropic–nematic transition is described exactly for very long rods. In addition to this exact limiting result, the calculation also provides an intuitive explanation for orientational ordering in a hard-particle fluid. The origin of the ordering transition lies in a competition between rotational and translational entropy: upon alignment, the system loses rotational entropy (i.e. becomes orientationally ordered); however, this loss is more than compensated by a gain in translational entropy in the aligned phase (due to a decrease in the particle pair excluded volume).

Here we give a brief synopsis of the Onsager calculation. Consider a fluid of N hard uniaxial monodisperse rods in a volume V. The degree of orientational order in this fluid is specified by the angular distribution function $h(\Omega)$, normalized such that $\int h(\Omega)\ \mathrm{d}\Omega = 1$, and $Nh(\Omega)\ \mathrm{d}\Omega$ gives the number of rods with orientations in the solid angle range $\Omega \to \Omega + \mathrm{d}\Omega$. The Helmholtz free energy F per rod, which is a functional of $h(\Omega)$,can be written as a sum of ideal mixing and excess configurational contributions (in units of $k_B T = 1/\beta$) as follows:

$$\beta F[h(\Omega)]/N = f^{\text{ideal}} + f^{\text{excess}}. \tag{2.1}$$

The ideal contribution is given by

$$f^{\text{ideal}} = \ln(\rho\Lambda^3) - 1 + \int h(\Omega)\ \ln[4\pi h(\Omega)]\ \mathrm{d}\Omega \tag{2.2}$$

where $\rho = N/V$ is the number density of rods and Λ is a constant arising from the single-particle partition function. This free-energy contribution favours an isotropic distribution of rods where $h(\Omega) = 1/4\pi$, in which case equation (2.2) reduces to the free energy of an ideal gas. The excess contribution to the free energy is considerably more difficult to calculate as it involves a $3N$-dimensional configurational integral. Onsager approximated this hard-rod excess configurational free energy using the second virial estimate

$$f^{\text{excess}} = \frac{\rho}{2} \int\int h(\Omega)h(\Omega')b^{\text{ex}}(\Omega, \Omega')\ \mathrm{d}\Omega\ \mathrm{d}\Omega' \tag{2.3}$$

where $b^{\text{ex}}(\Omega, \Omega')$ is the excluded volume between a pair of rods with orientations Ω and Ω'. (The pair excluded volume is the volume excluded to the centre of one particle by the presence of a second particle.) The exact form of $b^{\text{ex}}(\Omega, \Omega')$ depends on the geometry of the hard rods considered. For spherocylinders of diameter D and cylinder length L (particle volume $b_0 = \frac{1}{6}\pi D^3 + \frac{1}{4}\pi D^2 L$) the pair excluded volume is

$$b^{\text{ex}}(\Omega, \Omega') = 8b_0 + 2DL^2|\sin(\Omega - \Omega')|. \tag{2.4}$$

This pair excluded volume is at a minimum for parallel rods ($\Omega - \Omega' = 0$) and thus the excess free energy of equation (2.3) favours an orientationally ordered phase. Minimization of the Helmholtz free-energy functional (equation (2.1)) with respect to $h(\Omega)$, subject to the

normalization constraint on $h(\Omega)$, leads to a non-linear integral equation for the equilibrium orientation distribution function. Numerical solution of this equation shows that, with increasing density, the globally stable state switches from the isotropic to the nematic at $\rho = 4.55/(DL^2)$ and a first-order orientational ordering transition occurs in the hard-rod fluid [20]. This result is exact in the limit of $\rho \to 0$, $\rho DL^2 > 0$.

While the Onsager theory provides an intuitive understanding of entropically driven orientational ordering, this second virial approach is not quantitatively accurate for moderately asymmetric particles (for example, rods with $L/D < 50$) [21], and thus a theory that takes account of higher-order virial terms is required. An alternative approach, taken by Flory and DiMarzio, is the use of a lattice model, which reduces the calculation of the excess free energy to a combinatorics problem [22,23]. We will discuss these types of models in section 4.2. Another approach for describing hard-particle fluids, which is both simple and accurate, is provided by scaled particle theory [24,25]. The scaled particle calculation only requires the particle pair excluded volume as input and reduces to the Onsager result in the low-density limit. We make use of scaled particle theory in sections 4.3 and 5 of this review.

2.2. *Cell model for positional ordering*

The possibility of translationally ordered fluid phases in hard-particle systems has been, until quite recently, an open question. The fact that orientational ordering in hard-particle fluids can be understood in terms of a trade-off between rotational and translational entropy led us to surmise that translational order in such fluids may be stabilized by trade-offs between the three translational degrees of freedom. Starting from this intuitive idea we have developed a simple model for translationally ordered fluid phases in hard-particle systems [19]. In this model the periodic spatial distribution that characterizes these phases is imposed by the introduction of impenetrable cell boundaries. This enables us to separate the statistics for the translationally ordered dimensions of the system from the disordered or fluid dimensions. The ordered and disordered dimensions of the system remain coupled to each other through the effect that the spacing of the cell boundaries has on the entropy in each dimension. Here we outline the model in the context of a fluid of parallel hard spherocylinders for which recent computer simulation results are available [26,27].

We consider a fluid of N hard spherocylinders with axial ratio L/D, which are constrained to be parallel in a fixed volume V. In this system we consider the possibility of four distinct phases: the nematic phase, which is translationally disordered, and the smectic, columnar and crystal phases, which are translationally ordered. The periodic density modulations that define these ordered phases are created by dividing the system into appropriate types of cells with impenetrable boundaries. In the smectic phase, these boundaries are uniformly spaced parallel planes, which divide the system into layers such that the particles can freely interact with other particles in a layer, but interact only with the cell wall in the dimension perpendicular to the layer. In the columnar phase, space is divided into an array of tubes such that particles are free to move along the length of the tubes but may not penetrate into adjacent tubes. Finally in the crystalline phase, particles are individually confined to closed cells such that a particle interacts only with its cell walls on all sides. These artificial boundaries in essence divide space into separable ordered and disordered dimensions. In the $(3-d)$ ordered dimensions, each particle is alone in a $(3-d)$-dimensional box and the centre of the particle has a well defined set of allowed positions that keep the particle in the box. In the d disordered dimensions, the positions of the centres of the particles are constrained only by hard-core (excluded-volume) interactions

with other particles in the same cell and the behaviour is that of a d-dimensional fluid of d-dimensional hard particles.

This separation of disordered (fluid) and ordered (cell) dimensions enables us to construct a Helmholtz free energy of the following form:

$$\beta F_d/N = f^{\text{ideal}} + f_d^{\text{fluid}} + f_{3-d}^{\text{cell}} \tag{2.5}$$

where f_d^{fluid} is the excess free energy per particle of the appropriate d-dimensional fluid and f_{3-d}^{cell} is the excess free energy of complementary $(3-d)$-dimensional particles in $(3-d)$-dimensional cells. The nematic, smectic, columnar and crystal phases are specified in equation (2.5) by the labels $d = 3, 2, 1, 0$ respectively and f_0^{fluid}, $f_0^{\text{cell}} \equiv 0$. The excess fluid and cell contributions to the free energy are coupled in both the smectic and columnar phases through their mutual dependence on the smectic layer spacing and the columnar tube width, respectively. We use d-dimensional scaled particle theory [24] to evaluate f_d^{fluid} and a self-consistent free-volume cell model [28] to evaluate f_{3-d}^{cell}. By computing the free energy of equation (2.5) for each of the four phases as a function of density and axial ratio, a number of phase transitions can be located in this system. The resulting ρ versus L/D phase diagram displays regions of nematic, smectic, columnar and crystalline stability. This calculated phase diagram for parallel hard spherocylinders is in general agreement with computer simulation results [26, 27]. In section 5 we make use of this cell model to describe translational ordering in self-assembling systems.

3. The self-assembly process

3.1. Phenomenological description

A variety of molecules reversibly self-associate in solution to form structured molecular aggregates. The size distribution of these aggregates is generally very broad and the number of individual molecules or monomers comprising a distinct aggregate can range from two up to several thousand. This aggregation or association process is most commonly driven by the hydrophobic effect and the free energy of association per monomer is generally of the order of several k_BT [11, 29]. Thus the aggregates are actually in dynamic equilibrium with free monomers. The microscopic details of the association process are complex and vary from system to system. For example, in the case of micellar surfactants, free energies of self-assembly depend upon interactions between hydrophilic head-groups, solvation effects and the packing of the hydrophobic chains [12, 13, 30]. Noting that such microscopic details are primarily functions of temperature and local aggregate geometry (e.g. surface curvature), we make use of a simple phenomenological model for aggregate assembly that is generally applicable to a variety of systems [31, 32].

In this phenomenological approach we assume that the free energy arising from interactions between monomers in an aggregate is a function only of temperature and the local aggregate geometry and is independent of the individual aggregate size and the overall solute concentration. In the simplest case of linear aggregation, where aggregates comprise stacks of monomers, we introduce a single temperature-dependent parameter $-\phi(T)k_BT$ as the average free energy of association per monomer–monomer contact in such an aggregate. The free energy of association for a linear aggregate composed of n monomers (an n-mer) is thus $-(n-1)\phi(T)k_BT$. For a more general case of aggregation where monomers can form spherical, rod-like and disc-like aggregates (as in many micellar systems), we introduce a different phenomenological parameter for each local aggregate geometry. Assuming a

model in which all possible aggregate shapes can be divided into spherical, cylindrical and planar regions, we define the corresponding average free energies per monomer of intra-aggregate interactions in each of these regions as $-\Phi_0(T)k_BT$, $-\Phi_1(T)k_BT$ and $-\Phi_2(T)k_BT$, respectively†

3.2. Ideal-solution behaviour

Here it is instructive to consider the simple case of linearly self-assembling aggregates in the absence of inter-aggregate interactions (i.e. in ideal-solution conditions). This example will both demonstrate the above model for aggregate assembly and enable us to introduce some necessary formalism. In section 2.1 we introduced the orientational distribution function $h(\Omega)$, which described the orientational order in a system of monodisperse rods. In the analogous self-assembling system of rod-like aggregates we have a polydisperse distribution of rods and thus require a distribution function that accounts for both aggregate size and orientation. For this purpose we define the number concentration of n-mers in the orientation range $\Omega \rightarrow \Omega + d\Omega$ as $c_n(\Omega)$. This distribution function is constrained by the requirement that the total volume fraction of solute, given by

$$v_p = b_1 \sum_{n=1}^{\infty} \int n c_n(\Omega)\, d\Omega \tag{3.1}$$

where b_1 is the volume of a monomer, be fixed. In the absence of inter-aggregate interactions, the Helmholtz free energy is simply given by the sum of an ideal mixing and an association contribution as follows:

$$\beta F^{\text{ideal}}[c_n(\Omega)]/V = f^{\text{mix}} + f^{\text{assoc}} \tag{3.2}$$

where

$$f^{\text{mix}} = \sum_{n=1}^{\infty} \int d\Omega\; c_n(\Omega)\left\{\ln[4\pi\Lambda^3 c_n(\Omega)] - 1\right\} \tag{3.3}$$

and

$$f^{\text{assoc}} = -\sum_{n=1}^{\infty} \int d\Omega\; c_n(\Omega)(n-1)\phi. \tag{3.4}$$

The constant Λ in equation (3.3) refers to single-particle properties of the monomer‡ Note that equations (3.2)–(3.4) are given in terms of free energy per unit volume (i.e. free-energy density), which, for these self-assembling systems, is more convenient than the free energy per particle. The ideal mixing contribution to the free energy favours a large number of small aggregates while the association contribution favours a small number of large aggregates. This competition will lead to a well defined equilibrium size distribution of aggregates.

† These energies are equivalent to the 'standard' chemical potentials per monomer generally used in describing micelle assembly: $\Phi_0 = (\tilde{\mu}_1^0 - \tilde{\mu}_{\text{sphere}}^0)/k_BT$, $\Phi_1 = (\tilde{\mu}_1^0 - \tilde{\mu}_{\text{rod}}^0)/k_BT$, $\Phi_2 = (\tilde{\mu}_1^0 - \tilde{\mu}_{\text{plate}}^0)/k_BT$, where $\tilde{\mu}_1^0$, $\tilde{\mu}_{\text{sphere}}^0$, $\tilde{\mu}_{\text{rod}}^0$ and $\tilde{\mu}_{\text{plate}}^0$ are the 'standard' chemical potentials of a monomer in dilute solution, and in a spherical, rod-like or plate-like micellar region respectively (see e.g. [32]).

‡ McMullen *et al* [33] argue that the single-particle properties of aggregates, rather than monomers, should be considered in models of micellar systems. In this case the factor Λ in equation (3.3) is a function of aggregation number n and the ideal-solution size distribution is no longer a simple exponential as in equation (3.7).

The equilibrium distribution is determined by minimizing the free-energy functional with respect to the aggregate size and orientation distribution function as given by the following extremum condition:

$$\left.\frac{\delta\{\beta F[c_n(\Omega)]/V + \chi v_p[c_n(\Omega)]\}}{\delta c_n(\Omega)}\right|_{V,T,c_{n'}(\Omega')} = 0 \tag{3.5}$$

where χ is a Lagrange multiplier conjugate to the constraint of a fixed solute volume fraction. This minimization equation immediately leads to the following condition of multiple equilibria between distinct aggregate species, which characterizes reversibly self-assembling systems [34]:

$$\beta\mu_n(\Omega) = \left(\frac{\partial \beta F/V}{\partial c_n(\Omega)}\right)_{V,T,c_{n'}(\Omega')} = -\chi n b_1 = n\beta\mu_1(\Omega) \tag{3.6}$$

where $\beta\mu_n(\Omega)$ is the chemical potential of an Ω-oriented n-mer and the chemical potential of the unaggregated monomeric species is simply $\beta\mu_1(\Omega) = -b_1\chi$. Application of this extremum condition to the free-energy functional of equation (3.2) leads to the following orientationally isotropic equilibrium distribution function:

$$c_n(\Omega) = c_1(\Omega)\ \exp\left[-(n-1)\left(b_1\chi - \phi\right)\right] = \left(e^{-\phi}/4\pi\Lambda^3\right)\left(1 - 1/\langle n\rangle\right)^n \tag{3.7}$$

where $\langle n\rangle$ is the average aggregation number given by

$$\langle n\rangle = \tfrac{1}{2}\left\{1 + \left[1 + \left(4\Lambda^3/b_1\right)v_p e^{\phi}\right]^{1/2}\right\}. \tag{3.8}$$

For strong aggregation equation (3.8) reduces to the well known form $\langle n\rangle \sim (v_p e^{\phi})^{1/2}$. The function given in equation (3.7), known in polymer statistics as the 'most probable distribution' [35], is an exponentially decreasing function of aggregate size. For such a distribution, polydispersity increases with increasing $\langle n\rangle$ and the average aggregate size increases monotonically with both increasing concentration (v_p) and increasing association free energy (ϕ).

An analogous ideal-solution distribution function can readily be computed for micellar systems. In micellar systems, cooperative monomer association first occurs at the critical micelle concentration (CMC), which is the lowest concentration at which 'minimum' aggregates are thermodynamically stable [10–13]. These minimum aggregates are usually spherical in shape and composed of a nearly fixed number of monomers. With increasing concentration these minimum aggregates can grow into rod-like and/or disc-like micelles. For a rod-like micellar system we can describe the aggregate size and orientation distribution as above through a uniaxial number density $c_n(\Omega)$, where an aggregation number of $n = 1$ corresponds to unaggregated monomer, $n = n_0$ corresponds to minimum aggregates and $n > n_0$ corresponds to rod-like aggregates. Here we assume that there are no stable aggregates in the range $1 < n < n_0$. It is convenient to model a rod-like aggregate as a spherocylindrical n-mer such that n_0 monomers comprise the two hemispherical end-caps and the remaining $(n - n_0)$ monomers make up the cylindrical body. Defining the average free energy of association per monomer in the spherical and the cylindrical regions as $-\Phi_0(T)k_BT$ and $-\Phi_1(T)k_BT$, respectively, the total association free energy per unit volume for such a rod-like micellar system is given by

$$f^{\text{assoc}} = -\sum_{n=n_0}^{\infty}\int \mathrm{d}\Omega\ c_n(\Omega)\left[\left(n - n_0\right)\Phi_1 + n_0\Phi_0\left(1 - \delta_{1,n_0}\right)\right] \tag{3.9}$$

where $\delta_{m,n}$ is the usual Kronecker delta function. For the case of $n_0 = 1$ the previously discussed linear aggregation result (equation (3.4)) is recovered.

In ideal-solution conditions, the complete Helmholtz free-energy density for the micellar rod-like system is given by the sum of equations (3.3) and (3.9). The ideal equilibrium size distribution is obtained by functional minimization of this free-energy density (equation (3.5)) and depends on the two association parameters Φ_0 and Φ_1. The parameter Φ_0 gives a measure of the stability of the minimum aggregate and is related to the mole fraction at the CMC of the system through the approximate relation $X_{CMC} \sim \exp(-\Phi_0)$. In the limit of large Φ_0 the minimum aggregate is completely stable and essentially all monomers are associated into minimum or larger aggregates. In this case the behaviour of the system is completely governed by the difference $\Phi_1 - \Phi_0$ and the system resembles the simple linear aggregation system with the minimum aggregate playing the role of 'monomer' [31, 32, 36]. When Φ_0 is small compared to Φ_1, assembly is cooperative, with an abrupt transition from monomers to long aggregates, with increasing concentration.

4. Orientational ordering in surfactant and protein systems

In the absence of inter-aggregate interactions, there is no driving force for liquid-crystalline ordering and thus the self-assembled system remains orientationally isotropic. A model appropriate for the description of liquid-crystalline ordering in crowded self-assembling systems is obtained by adding an excess configurational free-energy contribution to the ideal mixing and association contributions accounted for in equation (3.2), i.e.

$$\beta F[c_n(\Omega)]/V = f^{mix} + f^{assoc} + f^{excess}. \tag{4.1}$$

For lyotropic systems, the excess free energy is dominated by a hard-core configurational contribution f^{config}, and additional soft interactions can be treated as perturbations to the hard-core reference. As noted in section 2 there are a number of theoretical approaches available for estimating f^{config}. For the self-assembling systems an approach that can be generalized to describe polydisperse and possibly polymorphic systems is required. In the following, we discuss orientational ordering in a variety of self-assembling systems using the free-energy functional of equation (4.1) with three different approaches for calculating f^{config}. The resulting aggregate size distributions maintain an exponential form, similar to equation (3.7), in both the isotropic phase and in each direction in the orientationally ordered phases, where the size distribution varies with orientation.

4.1. Second virial description

The second virial description of a monodisperse hard-rod fluid was outlined in section 2.1. This approach can be generalized to describe a polydisperse system of self-assembling rod-like aggregates. For example, in the linear and rod-like micellar self-assembling systems discussed in section 3.2, the second virial estimate of the excess configurational free energy per unit volume is given by

$$f^{config} = \tfrac{1}{2}\sum_{n=1}^{\infty}\sum_{n'=1}^{\infty}\int d\Omega \int d\Omega'\, c_n(\Omega)c_{n'}(\Omega')b^{ex}_{n,n'}(\Omega, \Omega') \tag{4.2}$$

where $b^{ex}_{n,n'}(\Omega, \Omega')$ is the pair excluded volume between an n- and an n'-mer in orientations Ω and Ω', respectively. Equation (4.2) is the polydisperse generalization of the monodisperse result of equation (2.3).

This second virial approach has been utilized by McMullen *et al* to describe orientational ordering in a self-assembling system of micellar rod-like aggregates [37]. These authors model the micellar aggregates as hard spherocylinders, with a minimum aggregation number $n_0 = 20$, and construct a Helmholtz free-energy functional that is equivalent to equation (4.1), with the ideal mixing, association and configurational contributions given by equations (3.3), (3.9) and (4.2), respectively (see second footnote in section 3.2). The equilibrium size and orientation distribution function is determined via the functional minimization of this free energy (equation (3.5)). As the second virial approach is valid only for dilute conditions, these authors limit their study to cases of strong aggregation, for which the isotropic–nematic transition occurs at low volume fractions. For the aggregation free energies considered, the isotropic–nematic transition occurs at a volume fraction ranging from 0.008 to 0.120, with the corresponding average aggregate axial ratio $\langle L/D \rangle$ at the isotropic phase boundary ranging from 360 to 22. At this transition, a strong coupling between aggregate growth and alignment is observed, with the average aggregate size being larger, and the size distribution more polydisperse, in the nematic phase, compared with the coexisting isotropic phase. In these coexisting phases it is found that the quantity $c_p \langle L \rangle^2 D$ is nearly constant, being equal to 3.7 in the isotropic phase and 5.0 in the nematic phase (where c_p is the total number density of aggregates).

The second virial approach of McMullen *et al* is expected to be quantitatively accurate in the dilute regime. However, micellar systems and many self-assembling protein systems generally form liquid-crystalline phases at volume fractions exceeding 10% [38–43, 17]. To address these systems we require an approximation for the configurational free energy that remains accurate (and mathematically tractable) beyond the dilute regime. To this end, we pursue both a lattice model and a scaled particle theory approximation in the following sections.

4.2. Lattice models

Lattice descriptions of hard-particle fluids are attractive since these models reduce the task of evaluating a $3N$-dimensional hard-particle configurational integral to a tractable combinatorics problem. This is especially advantageous when dealing with a polydisperse and heterogeneous population of particles such as that found in a self-assembled micellar solution. The price to be paid for this simplified approach is the lattice discretization of particle positions and orientations. Various approaches have been suggested for overcoming these limitations. For example, Flory's lattice model attempts to overcome the discrete orientation limitation by breaking particles up into segments and arranging the segments in staggered configurations to approximate particle orientations not parallel to the lattice directions [22]. On the other hand Herzfeld's lattice model [44, 45], which is a generalization of DiMarzio's model [23], attempts to overcome the discrete position limitation by using an underlying lattice that can be refined to a continuum limit. Here we make use of Herzfeld's model, which is especially suited for populations of particles that are polydisperse in width as well as length. While this model restricts particle orientations, we demonstrate at the end of this section that, for self-assembling systems, this approximation is not as severe as it appears [46].

We first address the simple linear aggregation system [47] discussed in section 3.2. We consider a polydisperse collection of self-assembling rod-like aggregates on a simple cubic lattice of volume V. The basic aggregating unit or monomer is a cube of edge length a (monomer volume $b_1 = a^3$), n of which can linearly aggregate to form a square rod of dimensions $a \times a \times na$. The system is described in terms of the size and orientation distribution function $c_n(\Omega_i)$, which gives the number density of n-aggregates in orientation

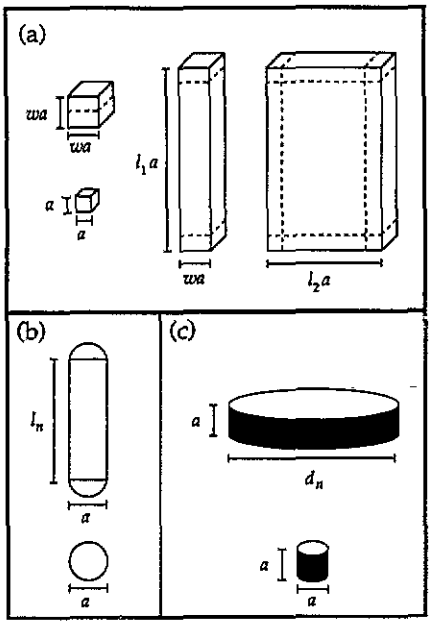

Figure 1. Schematic representation of the various aggregate geometries considered in this review. (*a*) In the lattice systems (section 4.2) cubic monomers self-assemble to form cubic minimum aggregates (with minimum aggregation number $n_0 = w^3$), uniaxial rectangular rod-like aggregates and biaxial plate-like aggregates. (*b*) In the linear aggregation rod-like system (section 5.1) spherical monomers self-assemble to form spherocylindrical rod-like aggregates and (*c*) in the simple disc-like system (section 5.3) symmetric right cylindrical monomers self-assemble to form disc-like aggregates.

Ω_i, where Ω_1, Ω_2, Ω_3 correspond to the three lattice directions. Equations (3.3) and (3.4) are applicable to this system if the integrations over Ω are converted to sums over Ω_i and the constant $4\pi\Lambda^3$ is replaced by ϵ^3, where ϵ is the refined lattice mesh spacing. The Helmholtz free-energy density in equation (4.1) is here a functional of the discrete size and orientation distribution function $c_n(\Omega_i)$. The excess configurational free-energy density for this lattice system is given by the following relatively simple expression:

$$f^{\text{config}} = -c_p \ln(1 - v_p) + \sum_{i=1}^{3} \alpha(\Omega_i)\lambda(\Omega_i) \tag{4.3}$$

where c_p is the total number density of aggregates, $\alpha(\Omega_i)$ is the total particle surface area per unit volume facing lattice direction Ω_i and $\lambda(\Omega_i)$ is the total particle length per unit volume along lattice direction Ω_i. Minimization of the complete Helmholtz free-energy density (equation (4.1)), for a given aggregation free energy ϕ and volume fraction v_p, via equation (3.5) yields the equilibrium aggregate size and orientation distribution function.

The phase diagram resulting from this calculation is shown in figure 2(*a*). Assuming that the aggregation free energy ϕ varies inversely with temperature, this figure can be interpreted as a temperature–concentration phase diagram. At very low aggregation free energies ($\phi < 5$), corresponding to high temperatures, there is insufficient aggregate growth to drive the formation of a liquid-crystalline phase. As the strength of aggregation is increased, aggregate growth is enhanced and a high concentration nematic phase is observed. With further increase in ϕ (lowering of the temperature) the alignment transition moves to lower volume fractions and the coexisting isotropic and nematic phases are separated by a relatively broad two-phase region. Finally, at large aggregation free energies ($\phi > 20$) aggregation is very strong and highly elongated aggregates form a nematic phase at very low concentrations. Details of the average aggregate size are given in figure 2(*b*) for the specific ϕ values. At low volume fractions, where the system is orientationally isotropic, the average rod length is larger here than in the corresponding ideal-solution case, indicating

that the inclusion of excluded-volume effects tends to promote aggregation in the isotropic phase [48]. At the isotropic–nematic transition there is a bifurcation in the average rod length between the different lattice directions as rods in the preferred direction grow at the expense of rods in the other two directions. A strong aggregate growth–alignment coupling is apparent with aggregates in the nematic phase being significantly longer than those in the coexisting isotropic phase.

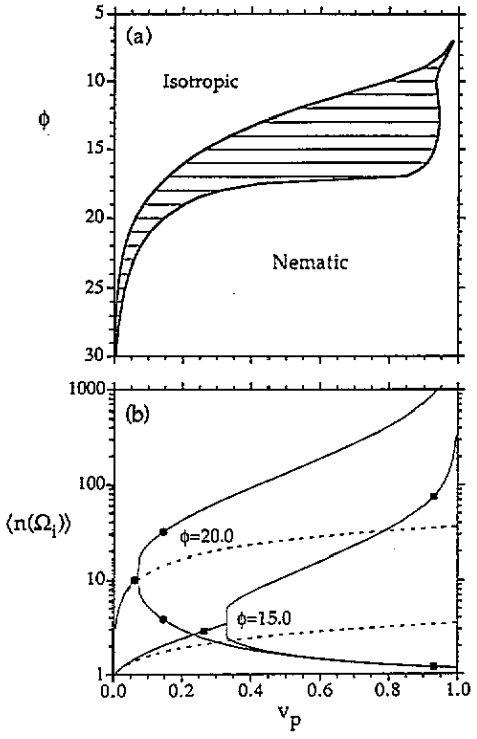

Figure 2. (*a*) Phase diagram for the n_0 = 1 linearly aggregating system and (*b*) associated average aggregation numbers for non-ideal (——) and ideal (----) solution conditions. The tie lines in (*a*) connect the coexisting isotropic and nematic phases. The symbols in (*b*) locate the isotropic–nematic phase boundaries.

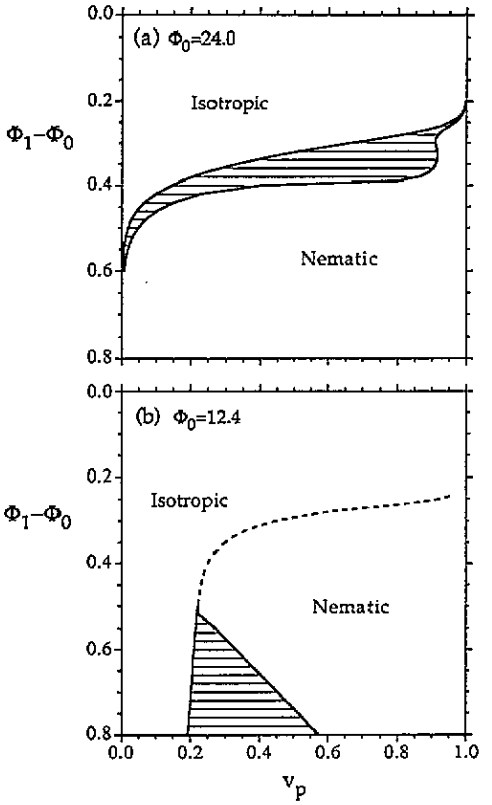

Figure 3. Phase diagrams for the n_0 = 64 micellar rod-like system in (*a*) the strong and (*b*) the weak aggregation limits. Tie lines connect the coexisting isotropic and nematic phases and the broken curve in (*b*) locates an apparently second-order alignment transition.

The linear aggregation process has only one degree of freedom for aggregate growth and the resulting phase behaviour is relatively simple. More complex phase behaviour can be expected from systems possessing multiple degrees of freedom in the aggregation process. For example, in a system of micellar rod-like aggregates we can consider regimes of strong, weak and intermediate aggregation strength. In the strong aggregation regime the minimum aggregate is very stable and the liquid-crystalline phase behaviour will be very similar to the case of simple linear aggregation. However, if the minimum aggregate is made progressively less stable, as is appropriate for certain self-assembling protein systems,

very different phase behaviour is possible. The second virial treatment of McMullen *et al*, described in section 4.1, was limited to the strong aggregation regime. Here we use our lattice model to study the micellar rod-like system in the strong, weak and intermediate aggregation regimes [47].

The polydisperse population of particles making up the rod-like micellar system consists of monomers, minimum aggregates and rod-like aggregates. In using a lattice model to compute the excess configurational free energy of this system, monomers are treated as cubes of edge length a, minimum aggregates as cubic assemblies of n_0 monomers with dimensions $wa \times wa \times wa$ ($n_0 = w^3$) and rod-like aggregates as rectangular rods of dimensions $wa \times wa \times la$ ($l > w$) (see figure 1(a)). This calculation is carried out on a refined lattice and thus, while the number of monomers comprising an aggregate must be an integer, the dimensions $w = n_0^{1/3}$ (which is fixed) and $l = (n/n_0)w$ (which is variable) are not required to take on integer values. As above, the size and orientation distribution of this self-assembling system is defined in terms of $c_n(\Omega_i)$, the number concentration of n-aggregates oriented in lattice direction i. The complete Helmholtz free-energy density for the micellar rod-like system is given by equation (4.1) with the ideal mixing and aggregate association contributions given by the lattice versions of equations (3.3) and (3.9), respectively, and the excess configurational contribution given by equation (4.3). For a given pair of aggregation free energies Φ_0 and Φ_1, and volume fraction, v_p, the equilibrium aggregate size and orientation distribution is given by the extremum condition of equation (3.5).

In figures 3(a) and (b) we show the resulting $\Phi_1 - \Phi_0$ versus v_p phase diagrams for both the strong and weak aggregation cases. Here we consider a system with a minimum aggregation number of $n_0 = 64$ and a refined lattice spacing of $\epsilon = 1/50$, values appropriate for the protein sickle-cell haemoglobin (HbS). As expected, the strong aggregation result ($\Phi_0 = 24.0$) shown in figure 3(a) is very similar to that of the simple linear aggregation system shown in figure 2(a) where the ordinates of these two diagrams are roughly related by $\phi \simeq n_0(\Phi_1 - \Phi_0)$. In contrast, the weak aggregation result ($\Phi_0 = 12.4$), shown in figure 3(b), is strikingly different. In this case the minimum aggregate is very unstable and the initial formation of aggregates (i.e. the CMC) is almost coincident with the alignment transition! In the phase diagram of figure 3(b) the isotropic phase boundary is nearly vertical for large values of $\Phi_1 - \Phi_0$ and the two-phase region rapidly narrows as this energy difference is decreased. At $\Phi_1 - \Phi_0 \simeq 0.50$ and $v_p \simeq 0.23$ there is an apparent multicritical point in the phase diagram where the isotropic–nematic transition changes from a discontinuous (first-order) transition to a continuous transition. With further decrease in $\Phi_1 - \Phi_0$ this continuous alignment transition moves to higher concentrations and disappears for $\Phi_1 - \Phi_0 < 0.20$. While this phase diagram may appear unusual, this type of phase behaviour is actually observed in the deoxygenated HbS system [49].

Finally, we consider the cases of intermediate Φ_0 values, which join the strong and weak aggregation limits. This is best done by considering a Φ_0 versus v_p phase diagram for fixed $\Phi_1 - \Phi_0$ as shown in figure 4. The phase boundaries labelled 'a' in this figure correspond to results shown in figure 3 for $\Phi_1 - \Phi_0 = 0.4$. For large values of Φ_0 (> 22) the system is in the strong aggregation regime and the phase behaviour is insensitive to changes in Φ_0 as evidenced by the chimney-like coexistence region in this portion of the phase diagram. As Φ_0 is decreased, the system enters an intermediate aggregation strength regime characterized by an extremely broad isotropic–nematic (and a limited nematic–nematic) coexistence region. With further decrease in Φ_0 (<13) the minimum aggregate becomes less stable, the CMC moves to higher volume fraction, and the isotropic–nematic two-phase region narrows rapidly, becoming vanishingly small at the apparent multicritical

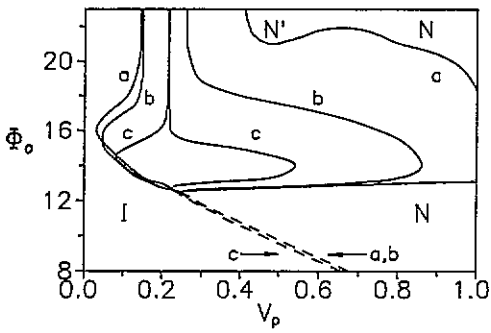

Figure 4. Phase boundaries for the $n_0 = 64$ micellar rod-like system with the addition of a repulsive step potential. This diagram is for a fixed value of $\Phi_1 - \Phi_0 = 0.4$. The pairs of full curves identify the coexisting isotropic (I) and nematic (N) phases for a first-order I–N transition while the broken curves identify an apparently second-order I–N transition. (*a*) Hard-core repulsions only as in figure 3: $\beta a^2 J = 0$, $\xi/a = 0$. (*b*) Short-range soft repulsions (e.g. elastic interactions): $\beta a^2 J = 0.1$, $\xi/a = 0.05$. (*c*) Longer-range soft repulsions (e.g. electrostatic repulsions): $\beta a^2 J = 0.1$, $\xi/a = 1.0$.

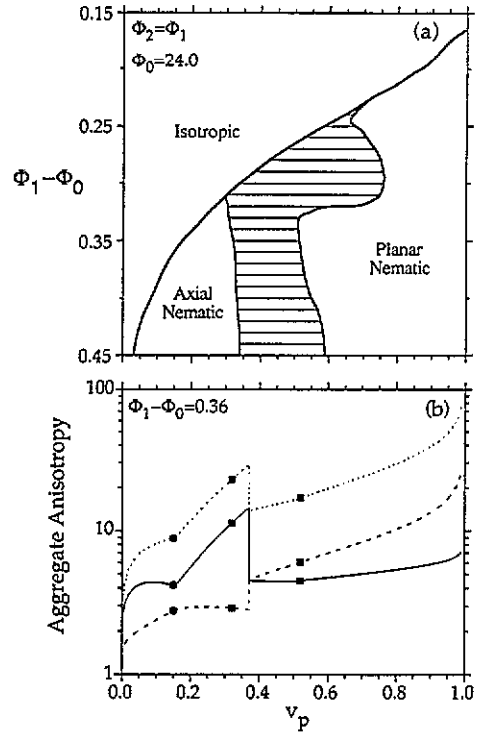

Figure 5. (*a*) Phase diagram for the $n_0 = 64$ general micellar system and (*b*) associated average aggregate anisotropies, $\langle l_{max}/w \rangle$ (·····), $\langle l_{mid}/w \rangle$ (----) and $\langle l_{max}/l_{mid} \rangle$ (——). These results are for the case when rod and plate growth are equally favoured. In (*a*) the tie lines connect coexisting phases and full curves separating pure phases indicate a very narrow first-order coexistence region. In (*b*) the symbols locate the isotropic–axial nematic transition (●) and axial nematic–planar nematic phase boundaries (■).

point. This is the weak aggregation regime.

The aggregate size distribution in many micellar systems is not limited to rod-like aggregates but may include disc-like or generally biaxial aggregates. The above model is easily extended to describe such polymorphic systems [45, 50]. In our lattice description of this more general micellar system we consider the possibility of biaxial plate-like aggregates, in addition to monomers, minimum aggregates and uniaxial rod-like aggregates. These biaxial particles are modelled as rectangular parallelepipeds of dimensions $wa \times l_1 a \times l_2 a$ (see figure 1(*a*)). In our above treatment of systems of uniaxial particles, the aggregation number n was sufficient to determine the geometry of a given aggregate. This is not the case for a system of biaxial aggregates and thus a more detailed aggregate size and orientation distribution function is required. For this purpose we define $c_{il_1l_2}$ as the number concentration of asymmetric aggregates with edge lengths wa, $l_1 a$ and $l_2 a$ oriented along lattice directions i, $i + 1$ and $i + 2$ respectively, where we employ the cyclic indexing convention $i + 3 \equiv i$ and require that $l_1 > w$ and $l_2 \geqslant w$. In this general micellar system

we consider monomers and minimum aggregates to be spherically symmetric objects, for which we introduce the orientation-independent number densities c_1 and c_{n_0}, respectively, where, as above, $n_0 = w^3$ is the minimum aggregation number. Thus the complete size and orientation distribution of this polydisperse and polymorphic system is specified by the set of number densities $c_t = \{c_1, c_{n_0}, c_{il_1l_2}\}$, where the label '$t$' refers to each distinct type (i.e. size and orientation) of particle. The Helmholtz free-energy density describing this system is given by equation (4.2) (here as a functional of c_t) with the lattice excess configurational contribution given by equation (4.3) and the ideal mixing and aggregate association contributions given as follows:

$$f^{\text{mix}} = \sum_t c_t\left[\ln\left(\epsilon^3 c_t\right) - 1\right] \tag{4.4}$$

$$f^{\text{assoc}} = -c_{n_0} n_0 \Phi_0\left(1 - \delta_{l,n_0}\right) - \sum_{i=1}^{3}\sum_{l_1>w}^{\infty}\sum_{l_2\geq w}^{\infty} c_{il_1l_2}\Big\{w^3\Phi_0 + w^2\left[\left(l_1 - w\right) + \left(l_2 - w\right)\right]\Phi_1 + w\left[\left(l_1 - w\right)\left(l_2 - w\right)\right]\Phi_2\Big\}. \tag{4.5}$$

The resulting equilibrium size and orientation distribution is given by an appropriately generalized version of equation (3.5).

This general micellar system displays a wide variety of phase behaviour depending upon the choice of the three aggregation free energies, Φ_0, Φ_1 and Φ_2 [50]. One of the most interesting cases is that of 'equally favoured rod and plate growth', i.e. $\Phi_2 = \Phi_1$. Under this condition purely steric and mixing considerations drive the system into either a rod-like or a plate-like state. The $\Phi_1 - \Phi_0$ versus v_p phase diagram for the $\Phi_2 = \Phi_1$ case is shown in figure 5(a). This diagram is computed for $\Phi_0 = 24.0$, $n_0 = 64$ and $\epsilon = 1/10$. For small values of $\Phi_1 - \Phi_0$ (<0.17) no liquid-crystal phases are formed. In the range $0.17 < \Phi_1 - \Phi_0 < 0.32$ there is a first-order transition from an isotropic phase to a nematic phase of planar symmetry. As this transition moves from high to intermediate concentrations, the initially very narrow coexistence region suddenly becomes quite broad. For $\Phi_1 - \Phi_0 > 0.32$ an axial nematic phase intervenes between the isotropic and the planar nematic phases. The first-order isotropic to axial nematic transition is via a very narrow coexistence region, while the subsequent first-order axial nematic to planar nematic transition is via a much broader two-phase region.

Details of the average aggregate dimensions for the case $\Phi_1 - \Phi_0 = 0.36$ are shown in figure 5(b). In this figure l_{max} and l_{mid} are defined as the maximum and middle aggregate dimensions, where $l_{\text{max}} \geqslant l_{\text{mid}} \geqslant w$, w being the minimum aggregate dimension. In the isotropic phase $\langle l_{\text{max}}\rangle$ and $\langle l_{\text{mid}}\rangle$ both increase monotonically and their relative values and rates of increase indicate that the system is initially composed of, on average, rod-like aggregates. The ratio $\langle l_{\text{max}}/l_{\text{mid}}\rangle$ also initially grows but at $v_p \simeq 0.05$ this quantity begins a slight decline, indicating that the aggregates are becoming, on average, slightly more plate-like. This trend is abruptly interrupted at the isotropic–axial nematic transition where $\langle l_{\text{max}}\rangle$ and $\langle l_{\text{max}}/l_{\text{mid}}\rangle$ both begin a rapid increase with increasing concentration while $\langle l_{\text{mid}}\rangle$ remains essentially constant. Through the axial–planar nematic transition the system undergoes a dramatic morphological reconstruction as the rod-like aggregates in the axial nematic phase change over to plate-like aggregates in the planar nematic phase. With further increase in concentration, both $\langle l_{\text{max}}\rangle$ and $\langle l_{\text{mid}}\rangle$ increase monotonically while $\langle l_{\text{max}}/l_{\text{mid}}\rangle$ remains fairly constant. These results demonstrate an essentially excluded-volume-driven transition of a rod-like system to a plate-like system. We note that, in terms of the symmetries of the

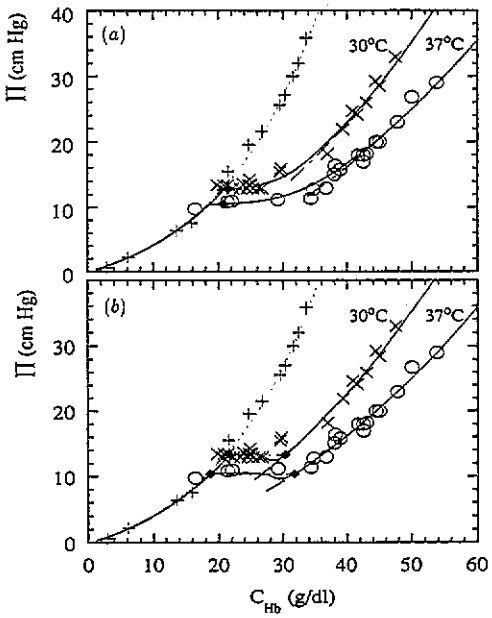

Figure 6. Osmotic pressure Π versus concentration C_{Hb} for solutions of deoxygenated sickle-cell haemoglobin. Symbols: experimental data for HbA (+) and for HbS at 37 °C (○) and 30 °C (×) [49]. Corresponding model results are given by the full and dotted curves. The results shown in (*a*) and (*b*) are for different strengths of the soft repulsive potential. In (*a*), where the repulsions are stronger, there is a very narrow biphasic region indicated by the diamonds (♦). In (*b*), where the repulsions are weaker, there is a broader biphasic region indicated by the pressure tie lines (♦----♦).

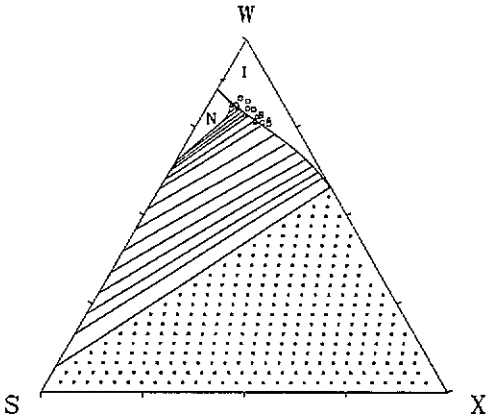

Figure 7. Ternary phase diagram for aqueous (W) solutions of mixtures of sickle-cell haemoglobin (S) with a hypothetical haemoglobin (X) that does not hybridize or aggregate. Tie lines connect coexisting isotropic (I) and nematic (N) phases. Points represent sedimentation data for pure HbS (*) and mixtures of HbS with HbA (□), HbA2 (△) and HbF (○) under non-hybridizing conditions [66]. The stippled region was numerically intractable.

aligned phases, the phase diagram of figure 5(*a*) is remarkably similar to the temperature–concentration phase diagram observed for many micellar surfactant systems. However, in these systems axial and planar orientational ordering are generally accompanied by hexagonal and lamellar translational ordering, respectively [38–40]. In section 5 of this review we take up the problem of translational order in reversibly self-assembling systems.

Thus far we have considered purely hard-core interaggregate interactions. Although this is a reasonable first approximation, for the types of association colloid systems we are considering, a more realistic interparticle potential would include a short-range soft repulsive component arising from elastic hydration or screened electrostatic forces. Hentschke and Herzfeld have introduced an additional soft repulsive step of width ξ and height J, where J has units of interaction energy per overlap area. (Note that a sum of such steps can be used to model any potential to the desired degree of detail.) A simple combinatorics analysis leads to the following expression for the self-repulsive free energy density of a

self-assembled system on a lattice

$$f^{\text{soft}} = \beta J \xi \sum_{i=1}^{3} \frac{[\alpha(\Omega_i)]^2}{1 - v_p + \xi\alpha(\Omega_i)}. \tag{4.6}$$

Inclusion of this soft repulsive potential into the model calculation (i.e. $f^{\text{excess}} = f^{\text{config}} + f^{\text{soft}}$ in equation (4.1)) can have significant effects on the resulting phase behaviour as seen in figure 4. In this figure, the phase boundaries labelled 'a' correspond to the strictly hard-core model ($\beta a^2 J = 0$) for the rod-like micellar system, with $\Phi_1 - \Phi_0 = 0.40$, $n_0 = 64$ and $\epsilon = 1/50$, considered previously. The phase boundaries labelled 'b' and 'c' are the results obtained for the same system with the addition of a soft repulsive potential to the hard-core interactions. The strength of the repulsive potential is taken as $\beta\alpha^2 J = 0.1$ and the range as $\xi a = 0.05$ and $\xi a = 1.0$ for phase boundaries 'b' and 'c' respectively. The primary effect of the soft repulsive interactions is to increase the osmotic pressure of the aggregates in the aligned hematic phase over the bare hard-core pressure. A magnification of this effect is seen in the phase diagram as the dramatic narrowing of the isotropic–nematic two-phase coexistence region in the strong and intermediate aggregation regimes. The soft repulsions have minimal effects on the phase diagram in the weak aggregation regime, as the nature and position of the multicritical point are essentially unaltered.

Finally, the validity of the discrete orientation approximation, inherent in the lattice model used above, has been investigated by Hentschke and Herzfeld for self-assembling systems [52]. These authors have derived a continuum expression for the configurational free energy that is a generalization of the lattice result given in equation (4.3). In the dilute limit this free-energy expression reproduces the second virial result given in equation (4.2). The phase diagrams computed from this full continuum model for the rod-like micellar system are qualitatively similar to the lattice-model phase diagrams presented here. Perhaps more importantly, the apparent multicritical point observed in the weak aggregation regime is still found in the continuum solution. In the following we continue to use the discrete orientation approximation [53], although we now dispense with the lattice model and turn to the much more accurate scaled particle treatment for the configurational free energy.

4.3. Scaled particle theory

Although the above lattice models go beyond the second virial approximation, they still significantly underestimate the effects of excluded volume at high packing densities. In order to make quantitative comparisons with experimental data for concentrated solutions, a more accurate theory is required. Scaled particle theory provides one approach that is particularly successful and simple to apply. Originally developed for the hard-sphere fluid by Reiss *et al* [24], the method has been successfully applied to the hard-rod fluid by Cotter and coworkers [25, 54] and to a hard-disc fluid by Savithramma and Madhusudana [55].

The scaled particle approach can be summarized quite succinctly. The quantity of interest is the work required to insert a test particle, whose dimensions are adjusted by a variable scaling parameter, into the hard-particle fluid. This work function can be computed exactly in the two extreme limits of an infinitesimally small and a macroscopically large scaled test particle. In the former limit, where three-body and higher interactions can be neglected, the work function is given rigorously by a second virial treatment, while in the latter limit, the work function is given directly in terms of the hydrostatic pressure resisting the formation of a macroscopic cavity in the fluid. By constructing an interpolation between these two limiting cases, the complete thermodynamics of the hard-particle fluid can be derived.

For the hard-sphere fluid a single scaling parameter is used to adjust the diameter of the scaled particle. The resulting equation of state is very accurate, being identical to the Percus–Yevick compressibility result. For hard spherocylinders, Cotter's version of scaled particle theory uses two scaling parameters as both the particle diameter D and length L are scaled independently. In this case, the results for spherocylinders compare well with the Monte Carlo equation of state [56] and with experimental osmotic pressure data for solutions of rod-like polymers (with persistent flexibility taken into account as necessary for the longer polymers) [57, 58]. Application of scaled particle theory to self-assembling systems requires adaptation for a polydisperse collection of particles. The appropriate expressions have been obtained by Cotter and Wacker [54] for polydisperse spherocylinders, by Taylor and Herzfeld [59] for polydisperse right cylindrical discs, and by Taylor [60] for polydisperse spheroplatelets.

Substitution of the scaled particle expressions for f^{config} in equation (4.1) for self-assembling systems leads to a startling result: the full expression of the excluded volume at high packing densities drives essentially complete aggregation into a very small number of very long, highly aligned particles. With just a bare hard-core interparticle potential, this dramatic drop in the particle number concentration results in a concomitant collapse of the osmotic pressure. Thus the bare hard-core interparticle potential, when treated as completely as possible, predicts unrealistic behaviour for self-assembling particles. Clearly a more realistic potential is required for these systems and the most obvious requirement for lyotropic systems is a soft repulsive interaction. It is striking that simply including a weak f^{soft} contribution to the free energy of the form of equation (4.6) produces well behaved results, even when the excluded volume is treated by scaled particle theory. As noted earlier, a sum of such step potentials can be used to mimic a soft potential of any desired form.

The most comprehensive equation-of-state data for self-assembling systems at high concentrations are the osmotic pressure data for deoxygenated sickle-cell haemoglobin (HbS) due to Prouty *et al* [49] (figure 6). Deoxygenated sickle-cell haemoglobin reversibly aggregates at physiological concentration and temperature (~35 g dl^{-1}, 37 °C) into helical fibres, most commonly composed of seven double strands of monomers with interstitial water [61]. Since the interstitial water must be in equilibrium with the bulk water, the degree of hydration of the aggregates must be allowed to vary with the osmotic pressure. This requires a free energy of contact formation that depends on the degree of fibre hydration. For the data available, a simple linear dependence of Φ_1 and Φ_0 on hydration suffices [62]. Approximating the shapes of the monomers as cubes of width equal to the monomer diameter, the minimum aggregates as cubes of width equal to the aggregate diameter, and the larger aggregates as rectangular parallelepipeds with the same cross section, the predicted equation of state, using scaled particle theory to account for the hard-core excluded volume and a mean-field treatment to account for the soft interactions, agrees well with the experimental data through the entire concentration range, for appropriately chosen values of the model parameters [63].

The theoretical calculations provide interpretations for the interesting features of the HbS osmotic pressure curves (figure 6). At low to moderate concentrations, HbS is monomeric like normal adult haemoglobin (HbA) and shows the same osmotic pressure. The non-ideality of such monomeric haemoglobin solutions was previously accounted for by a scaled particle treatment of the excluded volume of the monomers [64]. At higher concentrations, the osmotic pressure curves for deoxy sickle-cell haemoglobin deviate sharply from the normal haemoglobin curve. This sudden reduction in the osmotic pressure is due to the cooperativity of assembly when Φ_0 is less than Φ_1. After the onset of aggregation, the

osmotic pressure remains approximately constant over a range of concentrations. This suggests the coexistence of two phases. However, the calculations show that the range of isotropic–nematic coexistence will be very narrow unless soft repulsions are weak ((*a*) versus (*b*) of figure 6). The extension of the osmotic pressure plateau beyond the range of isotropic–nematic coexistence is due to the opposing effects of aggregate growth, tending to reduce the osmotic pressure, and soft repulsions, tending to increase the osmotic pressure. The disappearance of the osmotic pressure plateau for weak aggregation (at lower temperatures not shown here) corresponds to a multicritical point at which the isotropic–nematic transition is predicted to become second-order due to the interplay between aggregate growth and alignment [47, 52]. Beyond the osmotic pressure plateau, the rise in the osmotic pressure is nearly linear with concentration. This anomalously low-order dependence on packing density indicates that the hard-core volume of the particles is shrinking due to fibre dehydration at high osmotic pressures. The theoretical fit to the data suggests that the fibre width quoted in the literature represents a relatively dehydrated fibre and that fibres in solution may be swollen by as much as 50% in diameter.

In the red blood cell, HbS does not always occur as a pure solution. Although for homozygous individuals the *in vivo* solution is nearly pure HbS, in heterozygous individuals, or individuals with persistent expression of foetal haemoglobin (HbF), HbS is mixed with haemoglobins that do not aggregate as readily. The hypothetical case in which the non-sickle haemoglobin (HbX) does not hybridize with the sickle haemoglobin and does not participate in aggregation is relatively easy to model [65]. Figure 7 shows the phase diagram calculated for such a ternary system using the same parameters used to fit the osmotic pressure data of pure HbS solutions in figure 6(*a*). The apex of the triangle corresponds to pure solvent. A straight line from the apex to the bottom corresponds to a haemoglobin solution of increasing concentration with a fixed HbS:HbX ratio. Along the left leg of the triangle, corresponding to a binary system of solvent and pure HbS, an isotropic solution consisting essentially entirely of monomers exists at low concentrations and a nematic solution consisting of long, aligned fibres exists at higher concentrations. Coexistence of the isotropic and nematic phases is restricted to a narrow range of conditions in the binary system. As HbX:HbS increases (i.e. the line from the apex swings away from the left leg towards the right leg), the isotropic phase is predicted to persist to higher concentrations, in good agreement with the experimental data for a variety of non-sickle haemoglobins [66]. However, over a wide range of higher concentrations, a dramatic demixing is predicted whereby an exceedingly concentrated nematic solution of aggregated HbS separates from the isotropic solution. This wide two-phase region is the result of excluded volume: the entropic cost of demixing is less than the entropic cost of packing quasi-spherical HbX molecules among rod-like HbS fibres. In real haemoglobin mixtures, the free-energy cost of incorporating the non-sickle haemoglobin in the HbS fibre may be less than either of the above.

5. Translational ordering in simple self-assembling systems

In the previous section we have focused exclusively on orientational ordering in self-assembling systems and have ignored the possibility of translationally ordered phases. This is in fact a serious shortcoming since, for most self-assembled systems, translationally ordered liquid-crystalline phases are more common than nematic phases [38–40]. In this section we return to the simplest self-assembling systems but now consider the possibility of translational order. We address the two cases of simple rod-like and disc-like aggregation. The phase behaviour of these two systems is found to be very similar. In each case, we compare our theoretical predictions to experimental results.

5.1. A model rod-like system [59,67]

The linearly aggregating rod-like system is modelled as a set of reversibly assembled polydisperse spherocylindrical rods. The basic aggregating unit is a spherical monomer of diameter a (monomer volume $b_1 = \frac{1}{6}\pi a^3$), n of which can self-assemble to form a spherocylindrical n-mer of the same diameter a and cylinder length $l_n = \frac{2}{3}(n-1)a$ (i.e. n-mer volume $b_n = nb_1$) (see figure 1(*b*)). The system is described by the uniaxial aggregate size and orientation distribution function $c_n(\Omega)$. The ideal mixing and the aggregate association free-energy densities are given by equations (3.3) and (3.4), respectively, where $-\phi k_B T$ is the association free energy per monomer–monomer contact within an aggregate. The inter-aggregate interaction is taken as a hard-core repulsion plus a short-range soft repulsive step. The contribution to the total free energy arising from the soft repulsions is determined using a first-order perturbation theory [68] and the resulting expression is similar to the lattice result given in equation (4.6).

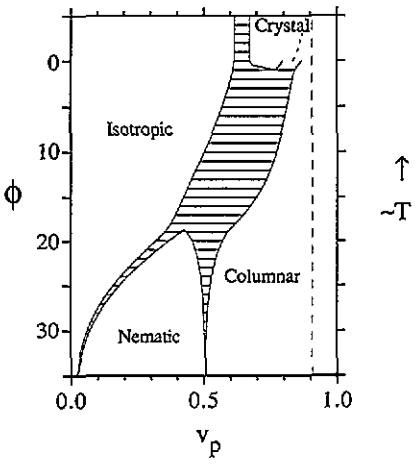

Figure 8. Phase diagram for the self-assembling rod-like system of section 5.1 calculated using model parameters given in the text. The tie lines connect coexisting phases while the vertical broken line indicates the hard-rod close-packing limit. The decreasing ϕ scale on the ordinate of this diagram can be interpreted as an increasing temperature scale.

As in the previous section we consider the possibility that an orientationally ordered nematic phase will be stable in this system. Additionally, we now consider the possibility that a translationally ordered columnar phase will also be stable. Smectic ordering, however, is not considered as we assume that such ordering will be suppressed due to aggregate polydispersity [69,70]. Finally, we consider the possibility of a high-concentration monodisperse crystal phase, which may be stable in the limit of very weak aggregation (i.e. small ϕ). The hard-core configurational free energy for the isotropic and nematic phases is computed using scaled particle theory as developed by Cotter and Wacker for a polydisperse population of spherocylindrical rods [54]. For the translationally ordered phases, the configurational free energy is constructed by generalizing the cell model presented in section 2.2. Thus we express the configurational free energy for the polydisperse columnar phase as the sum of a one-dimensional fluid contribution and a two-dimensional cell contribution. These two free-energy contributions are coupled through their mutual dependence on the column width Δ_c in the columnar phase. The one-dimensional fluid configurational free energy is computed using one-dimensional scaled particle theory (which yields the exact result) [24], while the cell configurational entropy is given by the ratio of the two-dimensional particle free volume to the two-dimensional cell volume. The configurational free energy of the monodisperse crystalline phase is computed using a three

dimensional self-consistent free-volume cell model [28]. The complete expressions for the hard-core free-energy density for these four phases (isotropic, nematic, columnar, crystal) are given in [59]. We solve this model in the discrete orientation approximation discussed in the previous section.

The predicted liquid-crystalline behaviour of the self-assembling rod-like system is shown in the ϕ versus v_p phase diagram of figure 8. The model parameters used in calculating this phase diagram are a monomer diameter of a = 12 Å and mass of m_l = 1000 amu, with a repulsive step potential of height βaJ = 1.0 and width ξ/a = 0.1. We note that the main qualitative features of figure 8 are not particularly sensitive to the choice of these parameters. The free energy of association ϕ is assumed to increase linearly with T^{-1}, corresponding to a negative enthalpy of aggregation. Thus figure 8 represents a temperature–concentration phase diagram.

The phase behaviour of figure 8 can be summarized as follows. There is a low-concentration isotropic phase whose region of stability grows with increasing temperature (weaker aggregation). A nematic phase is found to be stable at low temperatures in the concentration range 10–50%. With increasing temperature the narrow isotropic–nematic coexistence region moves to higher concentration until the nematic disappears at the isotropic–nematic–columnar triple point (v_p = 0.425, ϕ = 19.0). At a concentration of ~50% there is a low-temperature nematic–columnar transition via a narrow biphasic region and a high-temperature isotropic–columnar transition via a broad biphasic region. For most of the phase diagram the columnar phase is found to be stable out to close packing ($v_p \sim 0.9$). However, when aggregation is very weak (i.e. small ϕ or high temperature), the columnar phase becomes unstable with respect to a crystalline phase of monodisperse spheres or slightly anisotropic spherocylinders.

In addition to the macroscopic phase behaviour, our calculation also yields detailed information on the microscopic state of the self-assembled system. This includes average aggregate size, orientational order parameter and the inter-column spacing in the columnar phase. As expected, the average aggregate size increases monotonically with increasing concentration as well as with decreasing temperature. The average aggregate axial ratio $\langle l_n/a \rangle \simeq \frac{2}{3}\langle n \rangle$ at the isotropic–nematic transition is roughly given by $1/v_p^I$, where v_p^I is the volume fraction of the coexisting isotropic phase. In the columnar phase, the inter-column spacing is in the range $1.0 \leqslant \Delta_c/a \leqslant 1.2$ and is found to decrease with both increasing temperature and increasing concentration.

5.2. The TP6EO2M/water and related systems

A number of recent experimental investigations have been concerned with liquid-crystalline ordering in linearly aggregating self-association systems [4, 5, 71–73]. Much of this work is due to Boden and collaborators, who have studied both rod-like and disc-like systems. An ideal realization of a lyotropic self-assembling rod-like system is provided by the water soluble amphiphilic molecule 2,3,6,7,10,11-hexa-(1,4,7-trioxaoctyl)triphenylene (TP6EO2M), first synthesized by Boden *et al* [4]. The TP6EO2M molecule consists of a hydrophobic polyaromatic triphenylene core to which are attached six non-ionic hydrophilic ethyleneoxy side chains (molecular weight 936 amu, volume ~1500 Å^3, core diameter ~12 Å, maximum diameter ~23 Å). In aqueous solution, the molecules stack reversibly to sequester the triphenylene cores from the water environment. By design the TP6EO2M molecule is geometrically constrained to form only these rod-like aggregates.

The phase diagram of this system, determined from optical microscopy and deuterium NMR studies, is shown in figure 9. This experimental phase diagram is quite similar to the

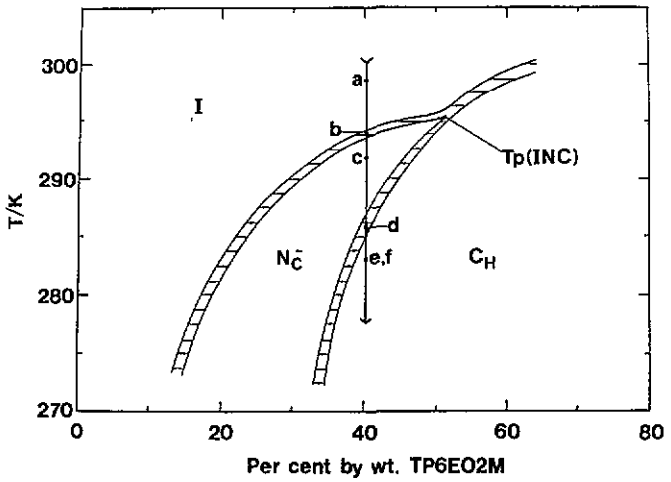

Figure 9. Experimental phase diagram for the rod-like self-assembling TP6EO2M/water system. The concentration scale is in units of amphiphile weight fraction, which, for this system, is roughly equivalent to solute volume fraction v_p. Phases are identified as I for isotropic, N_C^- for rod-like nematic and C_H for hexagonal columnar. Also identified is the isotropic–nematic–columnar triple point T_p(INC). The tie lines connect coexisting phases. (Reproduced with permission from Boden *et al* 1986 *Chem. Phys. Lett.* **123** 359 [4].)

model phase diagram of figure 8. In particular, both phase diagrams display an isotropic, nematic, columnar phase sequence at low temperatures. With increasing temperature the region of nematic stability narrows and finally terminates at an isotropic–nematic–columnar triple point. Above the triple point there is a direct first-order isotropic–columnar transition. In the experimental phase diagram (figure 9) the triple point occurs at a TP6EO2M weight fraction of 51% ($v_p \simeq 0.5$), while in the theoretical phase diagram (figure 8) the triple point is located at volume fraction of $v_p \simeq 0.425$.

In addition to the phase diagram, other experimental results are available for the TP6EO2M/water system. X-ray diffraction measurements have been carried out on such a system with a TP6EO2M weight fraction of 40% ($v_p \simeq 0.4$) in the isotropic, nematic and columnar phases. From these data average aggregation numbers are estimated (assuming a monodisperse aggregate size distribution) of $\langle n \rangle \simeq 6.5$ and $\langle n \rangle \simeq 7.8$ in the isotropic and nematic phases respectively. These values are comparable with our model results where $\langle n \rangle$ varies from ~3 to 10 at the isotropic–nematic transition in the neighbourhood of the triple point. The reduced aggregate number density, $\rho^* = c_p \langle l_n \rangle^2 a$, at this isotropic–nematic transition is found to be $\rho^* \simeq 0.3$, which is near our calculated value of $\rho^* \simeq 0.4$ in the vicinity of the figure 8 triple point. Finally, the experimentally measured columnar (hexagonal) spacing is $\Delta_c \simeq 31$ Å, which, combined with the estimates of monomer diameter, gives a relative columnar spacing in the range $1.3 \leqslant \Delta_c/a \leqslant 2.6$. In our model calculations the columnar spacing is found to be in the range $1.0 \leqslant \Delta_c/a \leqslant 1.2$.

While the TP6EO2M/water system is perhaps the best-studied linearly aggregating rod-like lyotropic system, phase diagrams for at least two other systems of this type have been determined. These are the disodium chromoglycate/water system studied by Hartshorne and Woodard [71] and others [5,72] and aqueous solutions of the tetrabenzocyclododecatetraene molecule substituted with eight methoxydiethylene oxide side chains studied by Zimmermann *et al* [73]. In both of these systems the planar amphiphilic molecules reversibly assemble by stacking to form linear rod-like aggregates.

The phase diagrams for these systems have the same general topology seen in figures 8 and 9 including the low-temperature isotropic, nematic, columnar phase sequence and the distinctive isotropic–nematic–columnar triple point. Finally, recalling that the linear aggregation model is applicable to rod-like micellar systems in the strong aggregation limit, our results suggest that the hexagonal phase formed by such systems comprises finite, as opposed to 'infinite', aggregates. Amaral *et al* have recently shown this to be true in the micellar sodium dodecyl lauryl sulphate/water system [74].

5.3. A model disc-like system [59]

We now turn to a simple disc-like system modelled as a set of reversibly assembled polydisperse right cylindrical discs. The basic aggregating unit is a symmetric right cylinder with height and diameter a (monomer volume $b_1 = \frac{1}{4}\pi a^3$), n of which can self-assemble to form a right cylindrical disc-like n-aggregate of height a and cylinder diameter $d_n = an^{1/2}$ (i.e. n-aggregate volume $b_n = nb_1$) (see figure 1(*c*)). This system can be described using a simple uniaxial aggregate orientation and size distribution function $c_n(\Omega)$. The ideal mixing and the aggregate association free-energy densities are given by equations (3.3) and (3.4), respectively. In using the association free energy of equation (3.4) we are implicitly ignoring edge effects [29, 32]. As with the rod-like system, the inter-aggregate interaction is taken as a hard-core repulsion plus a short-range soft repulsive step, with the latter treated as a first-order perturbation [68].

For this disc-like system we consider the possibility of a disordered isotropic phase, an orientationally ordered nematic phase and a translationally ordered smectic (lamellar) phase. We assume that columnar ordering will be suppressed by the disc polydispersity [69], although in the limit of very weak aggregation we do consider the possibility of a monodisperse columnar phase. The hard-core configurational free energy for the isotropic and nematic phases is computed using scaled particle theory applied to a system of polydisperse discs. This calculation is a generalization of Savithramma and Madhusudanas' treatment of monodisperse right cylinders [55]. The configurational free energy for the translationally ordered phases is constructed using a generalization of the cell model discussed in section 2.2. Thus, to describe the smectic phase, we consider a two-dimensional fluid of polydisperse circles representing discs confined within the one-dimensional cell corresponding to the thickness of a smectic layer. The two-dimensional fluid density and the one-dimensional cell entropy are coupled through their mutual dependence on the smectic layer spacing Δ_s. The two-dimensional fluid configurational free energy is computed using two-dimensional scaled particle theory [24], while the one-dimensional cell configurational entropy is given by the ratio $(\Delta_s - a)/\Delta_s$. The monodisperse columnar phase is treated in a manner analogous to the columnar phase of polydisperse rods described in section 5.1. The complete expressions for the hard-core configurational free-energy density for these four phases are given in [59]. As for the rod-like system, this disc-like model is solved in the discrete orientation approximation.

The phase diagram of the self-assembling disc-like system is shown, as a function of ϕ and v_p, in figure 10. The model parameters used in calculating figure 10 are a monomer diameter of $a = 9$ Å and mass of $m_1 = 500$ amu, with a repulsive step potential of height $\beta a^2 J = 0.2$ and width $\xi/a = 0.1$. As for the rod-like phase diagram of figure 8, the qualitative features of figure 10 are not particularly sensitive to the choice of these model parameters. Assuming ϕ increases linearly with T^{-1} (corresponding to a negative enthalpy of aggregation), figure 10 can be interpreted as a temperature–concentration phase diagram.

The phase behaviour of the self-assembling disc-like system (figure 10) is quite similar to that of the self-assembling rod-like system (figure 8). Again there is a low-concentration

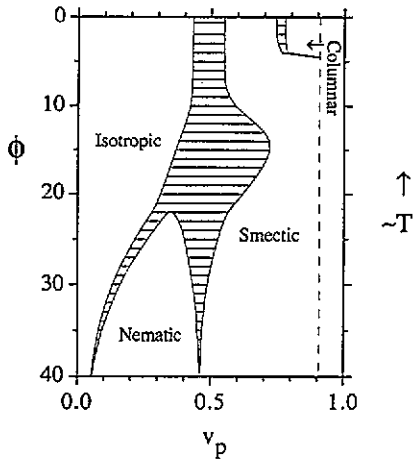

Figure 10. Phase diagram for the self-assembling disc-like system of section 5.3 calculated using model parameters given in the text. The tie lines connect coexisting phases while the vertical broken line indicates the hard-disc close-packing limit. The decreasing ϕ scale on the ordinate of this diagram can be interpreted as an increasing temperature scale.

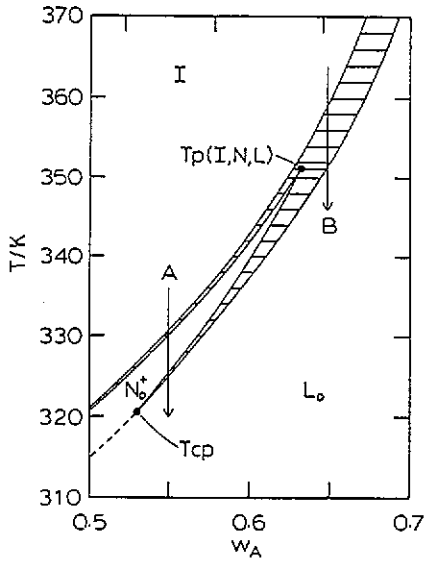

Figure 11. A selected portion of the experimental phase diagram for the disc-like self-assembling CsPFO/water system. The concentration scale is in units of amphiphile weight fraction w_A. For this system, the solute volume fraction is roughly given by $v_p \sim w_A/(2 - w_A)$. Phases are identified as I for isotropic, N_D^+ for disc-like nematic, and L_D for lamellar discs (smectic). Also identified are the triple point T_p(I,N,L) and a tricritical point T_{cp}. The tie lines connect coexisting phases while the broken curve indicates a second-order nematic–lamellar transition. (Reproduced with permission from Boden *et al* 1987 *J. Phys. Chem.* **91** 4092 [7].)

isotropic phase, whose range of stability grows with increasing temperature, and a high-concentration translationally ordered phase. In the case of self-assembled discs, the translationally ordered phase is smectic. Intervening between the isotropic and smectic phases at low-temperature is a nematic phase of polydisperse discs. With increasing temperature, the range of nematic stability narrows until it completely disappears at the isotropic–nematic–smectic triple point ($v_p \sim 0.35$, $\phi \sim 22.0$). For most of the temperature range of figure 10 the smectic phase is stable out to close packing ($v_p \sim 0.9$). However, at the highest temperatures, when aggregation is very weak, the smectic phase is replaced by a columnar phase of symmetric or slightly asymmetric monodisperse discs. (Note that a crystal of orientationally ordered right cylinders is never stable [26,27].)

In addition to the bulk phase diagram, we have computed, among other things, average aggregation numbers, orientational order parameters and the smectic layer spacing for this disc-like system. As in the case of the rod-like system, the disc-like aggregates grow with increasing concentration and decreasing temperature. Also, as for the rod-like system, the average aggregate axial ratio (d_n/a) at the isotropic–nematic transition is approximately given by $1/v_p^i$. The smectic layer spacing is found to be independent of temperature (i.e. independent of ϕ) and is in the range $1.0 \leqslant \Delta_s/a \leqslant 1.2$, decreasing with increasing concentration.

5.4. The CsPFO/water and related systems

As a model self-assembling disc-like lyotropic system, Boden's group has made an extensive study of the caesium perfluoro-octanoate (CsPFO)/water system [7]. The CsPFO molecule consists of a hydrophobic fluorocarbon chain attached to a hydrophilic caesium-carboxyl head-group (molecular weight 436 amu, volume ~360 Å^3, maximum dimension ~12.4 Å). The rigidity of the fluorocarbon chain, combined with the low hydration energy of the caesium head-group, causes this molecule to favour an aggregate geometry of minimal surface curvature, and in aqueous solution it forms discrete discoidal aggregates in all phases including the smectic.

A portion of the CsPFO/water phase diagram is shown in figure 11. The topology of this experimental phase diagram is quite similar to the theoretical disc-like phase diagram shown in figure 10. Most notably there is a low-temperature nematic phase intervening between a low-concentration isotropic phase and a high-concentration smectic phase. With increasing temperature the nematic region narrows and eventually disappears at an isotropic–nematic–smectic triple point, above which there is a direct isotropic–smectic transition. At the triple point, the isotropic, nematic and smectic phases coexist at volume fractions $v_p^I = 0.425$, $v_p^N = 0.431$ and $v_p^S = 0.448$, respectively, as compared with the calculated triple point in figure 9 at $v_p^I = 0.28$, $v_p^N = 0.36$ and $v_p^S = 0.55$. One interesting feature of the experimental phase diagram not found in our calculation is a nematic–smectic tricritical point where the nematic–smectic transition changes from first to second order with decreasing temperature. This omission is not surprising, however, since our somewhat crude cell description of the smectic phase precludes the possibility of a continuous transition from the nematic. However, we do find that the calculated nematic–smectic transition becomes more weakly first-order with decreasing temperature (increasing ϕ).

In addition to mapping out the phase diagram, the Boden group has carried out numerous other studies of the CsPFO/water system. These include x-ray diffraction and NMR quadrupolar splitting experiments at a number of temperatures and CsPFO concentrations. The x-ray diffraction studies indicate that CsPFO aggregates grow monotonically with decreasing temperature and increasing concentration. Typical discoid anisotropies in the nematic and smectic phases range from 1.8 to 4.3† Our theoretical results are in accord with this observed behaviour. In these x-ray studies, the reduced aggregate number density $\rho^* = c_p\langle d_n\rangle^3$ along the nematic–isotropic transition line is found to increase with temperature from 1.0 to 1.7. Our calculated values of ρ^* are in the range 1.3 to 1.8 along this transition line but they decrease with 'temperature'.

Estimates have also been made of the orientational order parameter S for the CsPFO/water system using both x-ray diffraction and NMR quadrupolar splitting data. The x-ray diffraction data for a CsPFO weight fraction of 55% ($v_p = 0.35$) give values of $S = 0.7$ at the nematic–isotropic transition and $S = 0.9$ at the nematic–columnar transition. The NMR quadrupole splitting data taken along the nematic–isotropic transition line indicate that S at the transition decreases with decreasing transition volume fraction. Both the large increase in S through the nematic phase at constant density (which is due to a growth–alignment coupling) and the decrease in S along the nematic phase boundary with decreasing transition volume fraction are seen in our model results.

Finally, a smectic (lamellar) layer spacing for the CsPFO/water system of $\Delta_s \simeq 42$ Å has been reported at $v_p = 0.35$ independent of temperature. Assuming a CsPFO aggregate thickness of $a = 22$ Å, this gives a scaled smectic layer spacing of $\Delta_s/a \simeq 1.9$, which is

† Photinos and Saupe [75] have questioned these results; however, see Boden and Jolley [76].

consistent with our theoretical construction of the smectic phase (which requires $\Delta_s/a < 2.0$) but is larger than our calculated smectic stability limit of $\Delta_s/a < 1.2$.

Boden's group has also made a detailed study of the ammonium PFO/water system [8] and find similar behaviour to the CsPFO/water system including a phase diagram nearly identical to figure 11. In addition to these two model systems, there are several other disc-forming lyotropics for which phase diagrams have been determined. These include aqueous solutions of the rigid-rod surfactant, caesium perfluoro-nonanoate [77], and a non-ionic amphiphile synthesized by Luhmann and Finkelmann [78], which consists of a flexible hydrophilic polyoxyethylene chain attached to a rigid hydrophobic biphenyl moiety. The phase diagrams for these two systems have the same general features seen in figures 10 and 11, including the low-temperature isotropic, nematic, smectic phase sequence and the characteristic isotropic–nematic–smectic triple point. Additionally, Herbst *et al* have established a partial phase diagram and carried out structural measurements for the tetramethylammonium perfluoro-nonanoate/water system [9]. They find the same low-temperature isotropic, nematic, smectic phase sequence and have determined that small disc-like aggregates comprise all three of these phases.

6. Conclusions

We have seen that the varying symmetries of the liquid-crystal phases of self-assembled molecular aggregates can be explained by the effects of excluded volume, modulated by soft repulsions. A phenomenological description of assembly, combined with a scaled particle treatment of excluded volume and a mean-field treatment of soft repulsions, suffices to obtain agreement with experimental data in cases ranging from surfactants to proteins, to polyaromatic amphiphiles. The extension to ternary and higher-order systems appears to be particularly promising.

However, there remain a number of outstanding issues that have yet to receive an adequate theoretical treatment. Among these, aggregate flexibility is perhaps the most important. In the case of monodisperse rods, flexibility can have dramatic effects on liquid-crystalline phase behaviour [79, 80]. In particular, very flexible hard rods do not form a nematic phase; rather they undergo a direct isotropic–columnar transition. In most micellar surfactant systems and for thin protein fibres, such as microfilaments, the persistence length of the aggregates is short compared to the length of the aggregates. In such cases, a rigid, hard-particle reference system does not adequately describe the configurational entropy of the aggregates. Odijk [81] and Hentschke [82] have partially addressed this problem for the case of linearly self-assembling aggregates that are constrained to be monodisperse. However, this work has yet to be extended to take polydispersity or non-linear assembly into account.

Another potentially problematic case is that of ionizable molecules far from their isoelectric pH [2, 3, 83]. If the ionic strength is not sufficiently high, the unscreened Coulomb interactions between charged aggregates may be strong enough that they cannot be treated in the mean-field approximation. However, the point may be irrelevant because unscreened Coulomb repulsions between charged monomers may prevent aggregate formation in the first place. In the case of proteins, unscreened Coulomb interactions within a monomer may cause unfolding (as seen in acid and base denaturation), in which case self-assembly is also moot. In any case, the present theory for liquid-crystalline phases of self-assembled molecular aggregates is best applied close to the isoelectric pH or at high ionic strengths.

These reservations aside, it is clear that we now have a substantial understanding of the microscopic basis for liquid-crystalline ordering in self-assembling systems. The pre-eminence of excluded-volume effects harks back to Onsager's work with monodisperse lyotropic systems over 40 years ago. The special features of the self-assembling systems are the extreme polydispersity of the labile particles and the coupling between the size distribution of the particles and the distributions of particle orientations and positions. These features are responsible for the rich phase behaviour that characterizes these systems.

Acknowledgments

We would like to thank Sow-Hsin Chen for suggesting that we write this review, and Reinhard Hentschke, Thomas Madden and Neville Boden for helpful discussions.

References

[1] Onsager L 1949 *Ann. NY Acad. Sci.* **51** 627
[2] Odijk T 1986 *Macromolecules* **19** 2313
[3] Vroege G J and Lekkerkerker H N W 1992 *Rep. Prog. Phys.* **55** 1241
[4] Boden N, Bushby R J and Hardy C 1985 *J. Physique Lett.* **46** L325
Boden N, Bushby R J, Hardy C and Sixl F 1986 *Chem. Phys. Lett.* **123** 359
Boden N, Bushby R J, Ferris L, Hardy C and Sixl F 1986 *Liq. Cryst.* **1** 109
[5] Attwood T K and Lydon J E 1984 *Mol. Cryst. Liq. Cryst.* **108** 349
Attwood T K, Lydon J E and Jones F 1986 *Liq. Cryst.* **1** 499
Attwood T K, Lydon J E, Hall C and Tiddy G J T 1990 *Liq. Cryst.* **7** 657
[6] Boden N, Bushby R J, Jolley K W, Holmes M C and Sixl F 1987 *Mol. Cryst. Liq. Cryst.* **152** 37
Boden N, Edwards P J B and Jolley K W 1993 *Structure and Dynamics of Strongly Interacting Colloids and Supramolecular Aggregates in Solution* ed S H Chen, J S Huang and P Tartaglia (Dordrecht: Kluwer)
[7] Boden N, Jackson P H, McMullen K and Holmes M C 1979 *Chem. Phys. Lett.* **65** 476
Boden N, Corne S A, Holmes M C, Jackson P H, Parker D and Jolley K W 1986 *J. Physique* **47** 2135
Holmes M C, Reynolds D J and Boden N 1987 *J. Phys. Chem.* **91** 5257
Boden N, Corne S A and Jolley K W 1987 *J. Phys. Chem.* **91** 4092
[8] Boden N, Clements J, Jolley K W, Parker D and Smith M H 1990 *J. Chem. Phys.* **93** 9096
[9] Herbst L, Hoffmann H, Kalus J, Reizlein K, Schmelzer U and Ibel K 1985 *Ber. Bunsenges. Phys. Chem.* **89** 1050
[10] Degiorgio V and Corti M (ed) 1985 *Physics of Amphiphiles: Micelles, Vesicles and Microemulsions* (Amsterdam: North-Holland)
[11] Tanford C 1980 *The Hydrophobic Effect* 2nd edn (New York: Wiley)
[12] Israelachvili J N, Mitchell D J and Ninham B W 1976 *J. Chem. Soc., Faraday Trans. II* **72** 1525
[13] Wennerstrom H and Lindman B 1979 *Phys. Rep.* **52** 1
[14] Yu L J and Saupe A 1980 *Phys. Rev. Lett.* **45** 1000
[15] Fujiwara F Y and Reeves L W 1980 *J. Phys. Chem.* **84** 653
[16] Holmes M C and Charvolin J 1984 *J. Phys. Chem.* **88** 810
[17] Harris J W 1950 *Proc. Soc. Exp. Biol. Med.* **75** 197
Stossel T P 1984 *J. Cell Biol.* **99** 15s
Hitt A L, Cross A R and Williams R C 1990 *J. Biol. Chem.* **265** 1639
[18] Darnell J, Lodish H and Baltimore D 1986 *Molecular Cell Biology* (New York: Scientific American Books)
[19] Taylor M P, Hentschke R and Herzfeld J 1989 *Phys. Rev. Lett.* **62** 800, 1577(E)
Hentschke R, Taylor M P and Herzfeld J 1989 *Phys. Rev.* A **40** 1678
[20] Herzfeld J, Berger A E and Wingate J W 1984 *Macromolecules* **17** 1718
[21] Frenkel D 1987 *J. Phys. Chem.* **91** 4912
[22] Flory P J 1956 *Proc. R. Soc.* A **234** 73
[23] DiMarzio E A 1961 *J. Chem. Phys.* **35** 658
[24] Reiss H, Frisch H L and Lebowitz J L 1959 *J. Chem. Phys.* **31** 369
Helfand E, Frisch H L and Lebowitz J L 1961 *J. Chem. Phys.* **34** 1037

[25] Cotter M A 1979 *The Molecular Physics of Liquid Crystals* ed G R Luckhurst and G W Gray (London: Academic) ch 7
[26] Stroobants A, Lekkerkerker H N W and Frenkel D 1986 *Phys. Rev. Lett.* **57** 1452; 1987 *Phys. Rev.* A **36** 2929
[27] Veerman J A C and Frenkel D 1991 *Phys. Rev.* A **43** 4334
[28] Hill T L 1956 *Statistical Mechanics* (New York: Dover) ch 8
[29] Israelachvili J N 1992 *Intermolecular and Surface Forces* (London: Academic)
[30] Puvvuda S and Blanckschtein D 1990 *J. Chem. Phys.* **92** 3710
[31] Blanckschtein D, Thurston G M and Benedek G B 1986 *J. Chem. Phys.* **85** 7268
[32] McMullen W E, Ben-Shaul A and Gelbart W M 1984 *J. Colloid Interface Sci.* **98** 523
[33] McMullen W E, Gelbart W M and Ben-Shaul A 1984 *J. Phys. Chem.* **88** 6649
[34] Hill T L 1964 *Thermodynamics of Small Systems* pt 2 (New York: W A Benjamin)
[35] Flory P J 1953 *Principles of Polymer Chemistry* (Ithaca, NY: Cornell University Press)
[36] Missel P J, Mazar N A, Benedek G B, Young C Y and Carey M C 1980 *J. Phys. Chem.* **84** 1044
[37] McMullen W E, Gelbart W M and Ben-Shaul A 1985 *J. Chem. Phys.* **82** 5616
[38] Tiddy G J T 1980 *Phys. Rep.* **57** 1
[39] Fontell K 1981 *Mol. Cryst. Liq. Cryst.* **63** 59
[40] Charvolin J and Sadoc J F 1991 *Physica* A **176** 138
[41] Rizzatti M R and Gault J D 1986 *J. Colloid Interface Sci.* **110** 258
[42] Radley K and Tracey A S 1985 *Mol. Cryst. Liq. Cryst. Lett.* **1** 95
[43] Boidart M, Hochapfel A and Laurent M 1988 *Mol. Cryst. Liq. Cryst.* **154** 61
[44] Herzfeld J 1982 *J. Chem. Phys.* **76** 4185
[45] Herzfeld J 1988 *J. Chem. Phys.* **88** 2776
[46] Straley J P 1972 *J. Chem. Phys.* **57** 3694
[47] Herzfeld J and Taylor M P 1988 *J. Chem. Phys.* **88** 2780
[48] Gelbart W M, Ben-Shaul A, McMullen W E and Masters A 1984 *J. Phys. Chem.* **88** 861
[49] Prouty M S, Schechter A N and Parsegian V A 1985 *J. Mol. Biol.* **184** 517
[50] Taylor M P, Berger A E and Herzfeld J 1988 *Mol. Cryst. Liq. Cryst.* **157** 489; 1989 *Mater. Res. Soc. Symp. Proc.* **134** 21; 1989 *J. Chem. Phys.* **91** 528
[51] Hentschke R and Herzfeld J 1989 *J. Chem. Phys.* **91** 7308
[52] Hentschke R and Herzfeld J 1989 *J. Chem. Phys.* **90** 5094
[53] Zwanzig R W 1963 *J. Chem. Phys.* **39** 1714
[54] Cotter M A and Wacker D C 1978 *Phys. Rev.* A **18** 2669
[55] Savithramma K L and Madhusudana N V 1981 *Mol. Cryst. Liq. Cryst.* **74** 243
[56] Frenkel D 1988 *J. Phys. Chem.* **92** 3280
[57] Hentschke R 1990 *Macromolecules* **23** 1192
[58] DuPre D B and Yang S 1991 *J. Chem. Phys.* **94** 7466
[59] Taylor M P and Herzfeld J 1991 *Phys. Rev.* A **43** 1892
[60] Taylor M P 1991 *Liq. Cryst.* **9** 141
Taylor M P and Herzfeld J 1991 *Phys. Rev.* A **44** 3742
Taylor M P unpublished notes
[61] Dykes G W, Crepeau R H and Edelstein S J 1979 *J. Mol. Biol.* **130** 451; 1978 *Nature* **272** 506
[62] Hentschke R and Herzfeld J 1990 *Mater. Res. Soc. Symp. Proc.* **177** 305
[63] Hentschke R and Herzfeld J 1991 *Phys. Rev.* A **43** 7019
[64] Ross P D and Minton A P 1977 *J. Mol. Biol.* **112** 437
[65] Madden T L and Herzfeld J 1992 *Mater. Res. Soc. Symp. Proc.* **248** 95
Madden T L and Herzfeld J 1993 to be published
[66] Benesch R E, Edalji R, Benesch R and Kwong S 1980 *Proc. Natl. Acad. Sci. USA* **77** 5130
[67] Taylor M P and Herzfeld J 1990 *Langmuir* **6** 911; 1990 *Mater. Res. Soc. Symp. Proc.* **177** 135
[68] Zwanzig R W 1954 *J. Chem. Phys.* **22** 1420
[69] Sluckin T J 1989 *Liq. Cryst.* **6** 111
Hentschke R unpublished results
[70] Stroobants A 1992 *Phys. Rev. Lett.* **69** 2388
[71] Hartshorne N H and Woodard G D 1973 *Mol. Cryst. Liq. Cryst.* **23** 343
[72] Goldfarb D, Labes M M, Luz Z and Poupko R 1982 *Mol. Cryst. Liq. Cryst.* **87** 259
Perahia D, Goldfarb D and Luz Z 1984 *Mol. Cryst. Liq. Cryst.* **108** 107
[73] Zimmermann H, Poupko R, Luz Z and Billard J 1989 *Liq. Cryst.* **6** 151
[74] Amaral L Q, Gulik A, Itri R and Mariani P 1992 *Phys. Rev.* A **46** 3548

[75] Photinos P and Saupe A 1990 *Phys. Rev.* A **41** 954
[76] Boden N and Jolley K W 1992 *Phys. Rev.* A **45** 8751
[77] Fontell K and Lindman B 1983 *J. Phys. Chem.* **87** 3289
[78] Luhmann B and Finkelmann H 1986 *Colloid Polym. Sci.* **264** 189
[79] Hentschke R and Herzfeld J 1991 *Phys. Rev.* A **44** 1148
[80] Selinger J V and Bruinsma R F 1991 *Phys. Rev.* A **43** 2922
[81] Odijk T 1987 *J. Physique* **48** 125
[82] Hentschke R 1991 *Liq. Cryst.* **10** 691
[83] Stroobants A, Lekkerkerker H N W and Odijk T 1986 *Macromolecules* **19** 2232